Bol. Soc. Paran. Mat.
©SPM – E-ISSN-2175-1188
SPM: www.spm.uem.br/bspm

(3s.) **v. 2026 (44) 8** : 1–23.
ISSN-0037-8712
doi:10.5269/bspm.79250

Wrapped Maxwell-Boltzmann Distribution: Properties and Application in Circular Statistics

Chinonso Michael Eze, Doaa M. H. Ahmed, Charity Uchenna Onwuamaeze, Eviano Israel Joel, Okechukwu J. Obulezi*, Ehab M. Almetwally and Mohammed Elgarhy

ABSTRACT: This paper introduces the Wrapped Maxwell-Boltzmann (WM-B) distribution, a novel circular probability model derived by wrapping the Maxwell distribution onto the unit circle. Through Poisson summation and subsequent normalization, the density is analytically simplified to its first-order form: a cosine perturbation of the circular uniform distribution. We derive its key distributional properties, including trigonometric moments, mean direction, circular variance, and entropy, and establish the non-negativity condition for the scale parameter as $\sigma \geq 0.2\pi$. Six methods for parameter estimation are investigated: Maximum Likelihood (MLE), Maximum Product of Spacings (MPSE), Least Squares (LS), Weighted Least Squares (WLS), Cramér von Mises (CvM), and Bayesian Estimation. Simulation studies demonstrate that the MPSE method is the most efficient for $\sigma = 0.75$, exhibiting the lowest bias and Root Mean Squared Error (RMSE). The model's empirical relevance is confirmed through application to two real-life datasets: wind direction and pigeon homing experiment data. For the wind direction data, the fitted parameter $\sigma = 2.23$ yielded a Watson goodness-of-fit p-value of 0.475, indicating model adequacy. The WM-B distribution offers a mathematically simple and practically effective tool, demonstrating superior or competitive performance against established circular models in practical applications.

Keywords: Circular, Wrapping, Maxwell-Boltzmann distribution, trigonometric moments, maximum product of spacings, first-order.

Contents

* Corresponding author.

Submitted September 29, 2025. Published March 12, 2026
2020 *Mathematics Subject Classification:* 62H11.

1. Introduction

The Maxwell-Boltzmann distribution is relevant in statistical physics with practical applications in modeling velocities (or energies) of particles in an ideal gas. It is a special case of the inverse Weibull distribution introduced by [10]. The distribution belongs to the Gaussian family ([15,17]) characterized by a scale parameter, σ. See related models, [29], [21], [22], [23], [24], [25], [26], [28], [27], and [30].

In probability theory, the study of random variables defined on the circle has become increasingly important in fields such as Meteorology, Geology, Physics, Biology, and Engineering (see, for example, [11,18,1,6]). Hence, Directional data analysis has emerged as an important area of statistics within the past few decades ([14]). Unlike linear random variables, circular random variables take values on the unit circle, which requires specialized probability models to capture their periodic nature ([8]).

A key method of constructing circular distributions is through the wrapping technique, where a linear distribution is projected onto the unit circle by taking values modulo 2π. The idea behind the wrapping approach is simple ([5,12]). Perhaps, this is the most popular technique for generating distributions around the unit circle, giving rise to a multitude of wrapped circular distributions ([7]). This approach has generated circular equivalence of some basic linear distributions such as the wrapped normal, wrapped Laplace, wrapped Cauchy, wrapped exponential distribution, etc ([3,13,4]). These distributions have application in areas involving directional data or phenomena with circular characteristics. Existing works on circular statistics have provided rich accounts of wrapped distributions ([13,3]). These models form the backbone of most applied directional analyses, with well-developed theoretical properties and estimation procedures.

[9] recently proposed a new circular distribution by wrapping the Lindley distribution and applied it for biological data. [2] introduced a new one-parameter circular distribution based on the wrapping method, called the wrapped modified Lindley distribution. The proposed model was applied to two real-life datasets, and its performance was compared with that of the wrapped Lindley, wrapped exponential and transmuted wrapped exponential models. [19] proposed an asymmetric semi-circular two-parameter model, termed the Semicircular Maxwell–Boltzmann distribution, specifically developed to represent posterior corneal curvature data, with its mathematical properties comprehensively derived.

However, despite the Maxwell-Boltzmann distribution's central role in classical statistical mechanics, its circular analogue, the wrapped Maxwell-Boltzmann distribution, has remained underexplored. Hence, a need for this study.

The wrapped Maxwell-Boltzmann distribution is derived by applying the periodic wrapping operation to the standard Maxwell-Boltzmann distribution. The wrapping process effectively converts the real-valued velocities into periodic variables, which are constrained within a fixed range, typically between 0 and 2π ([13,8]). The distribution can have applications in statistical physics, which involves dealing with angular components of velocity or particles restricted to move along circular or spherical domains. It can also be used in modeling neural activity, where the phase of oscillatory neurons can be described using a wrapped distribution.

Section 2 of this work deals with the derivation of the distribution, while Section 3 concentrates on its statistical properties. In Section 4, the maximum likelihood estimator of the unknown parameter is described. A simulation study is conducted in Section 5. In Section 6, the new model is implemented on both real-life data (wind direction and pigeon homing experiment data). The study is concluded in Section 7.

2. The Wrapped Maxwell-Boltzmann Distribution

A random variable X is said to follow a Maxwell distribution if the probability density function is given as

$$f(x) = \frac{\sqrt{2}}{\sigma^3\sqrt{\pi}} x^2 e^{-x^2/(2\sigma^2)}; \quad x \geq 0$$

This distribution is also commonly given as:

$$f(x) = \frac{2}{\pi\sigma^3} x^2 e^{-x^2/(2\sigma^2)}; \quad x \geq 0$$

We adopt the form:

$$f(x) = \frac{2}{\pi\sigma^3} x^2 e^{-x^2/(2\sigma^2)}; \quad x \geq 0$$

Where σ is the scale parameter. This distribution is ideally used in modeling the speeds of particles in gases, where the particles move freely in a stationary container without intersecting with one another. It is a distribution that has a wide application in physics. It plays a central role in statistical physics and is especially relevant in the kinetic theory of gases.

If a random variable X has a probability density function $f(x)$ with characteristic function, $\phi(t)$. Assuming that the linear random variable X is wrapped on the circumference of a unit circle, and the wrapped variables are denoted by θ. The relation between X and θ is expressed as

$$\theta = X \pmod{2\pi}$$

Conventionally, θ has a circular probability density function given as

$$f(\theta) = \sum_{k=-\infty}^{\infty} f(\theta + 2\pi k); \quad \theta \in [0, 2\pi) \tag{2.1}$$

Using the relation in equation (2.1), the wrapped Maxwell distribution with scale parameter σ is presented as

$$f(\theta) = \sum_{k=-\infty}^{\infty} \frac{2}{\pi\sigma^3} (\theta + 2\pi k)^2 e^{-(\theta+2\pi k)^2/(2\sigma^2)}; \quad \theta \in [0, 2\pi)$$

To evaluate the form further, we observe that each term includes a Gaussian-like function centered on integer multiples of 2π, which decays exponentially as k reduces from zero. This type of series is often tackled by using Poisson summation, which accounts for periodic Gaussian sums. Let,

$$f_k = (\theta + 2\pi k)^2 e^{-(\theta+2\pi k)^2/(2\sigma^2)}$$

Our interest is to compute $\sum_{k=-\infty}^{\infty} f_k$. The Poisson summation formula is used to evaluate infinite sums of Gaussian-like functions that are spaced periodically. The formula states:

$$\sum_{k=-\infty}^{\infty} f(\theta + 2\pi k) = \frac{1}{2\pi} \sum_{j=-\infty}^{\infty} \mathcal{F}(j) e^{ij\theta}$$

Where $\mathcal{F}(j)$ is the Fourier transform of f. While k indexes the periodic copies of f in the angular domain, j is the Fourier index (harmonic/frequency) in the Fourier series expansion. Let,

$$f(\alpha) = \alpha^2 e^{-\alpha^2/(2\sigma^2)}$$

where $\alpha = \theta + 2\pi k$. The Fourier transform of $f(\alpha)$ is

$$\mathcal{F}(j) = \int_{-\infty}^{\infty} \alpha^2 e^{-\alpha^2/(2\sigma^2)} e^{-ij\theta} d\alpha = 2\pi\sigma^3 \left(j^2 - \frac{1}{\sigma^2}\right) e^{-j^2\sigma^2/2}$$

Substitute $\mathcal{F}(j)$ into the Poisson summation formula and evaluate accordingly. Hence,

$$f(\theta) = \frac{2}{\pi\sigma^3} \sum_{k=-\infty}^{\infty} (\theta + 2\pi k)^2 e^{-(\theta+2\pi k)^2/(2\sigma^2)}$$

$$= \frac{2}{\pi\sigma^3}\frac{1}{2\pi}\sum_{j=-\infty}^{\infty} 2\pi\sigma^3\left(j^2 - \frac{1}{\sigma^2}\right)e^{-j^2\sigma^2/2}e^{ij\theta}$$

Thus,

$$f(\theta) = \frac{1}{\pi}\sum_{j=-\infty}^{\infty}\left(j^2 - \frac{1}{\sigma^2}\right)e^{-j^2\sigma^2/2}e^{ij\theta} \tag{2.2}$$

Equation (2.2) is a function of θ, σ, and π, and it leverages the periodicity of the Gaussian-modulated terms in the sum. However, it is not a probability distribution since it is not valid and non-negative for all θ. This prompts the need for further modification, as shown in the section below.

2.1. The first-order Wrapped Maxwell-Boltzmann Distribution

To show that equation (2.2) above is not a true probability density function, integrate it with respect to θ and evaluate over the support region, $[0, 2\pi)$.

$$\int_0^{2\pi} f(\theta)d\theta = \int_0^{2\pi}\frac{1}{\pi}\sum_{j=-\infty}^{\infty}\left(j^2 - \frac{1}{\sigma^2}\right)e^{-j^2\sigma^2/2}e^{ij\theta}d\theta$$

Since the series converges, we interchange the sum and the integral. Therefore,

$$\int_0^{2\pi} f(\theta)d\theta = \frac{1}{\pi}\sum_{j=-\infty}^{\infty}\left(j^2 - \frac{1}{\sigma^2}\right)e^{-j^2\sigma^2/2}\int_0^{2\pi} e^{ij\theta}d\theta$$

But the integral $\int_0^{2\pi} e^{ij\theta}d\theta$ is a standard result which is given as, $2\pi\delta_{j,0}$, where $\delta_{j,0}$ is the Kronecker delta function defined as $\delta_{j,0} = 1$ if $j = 0$, 0 otherwise. Hence,

$$\int_0^{2\pi} f(\theta)d\theta = \frac{1}{\pi}\sum_{j=-\infty}^{\infty}\left(j^2 - \frac{1}{\sigma^2}\right)e^{-j^2\sigma^2/2}2\pi\delta_{j,0}$$

Since $2\pi\delta_{j,0}$ is nonzero only when $j = 0$, the sum collapses to just the term where $j = 0$. Substituting $j = 0$ into the sum reduces the integral to

$$\int_0^{2\pi} f(\theta)d\theta = \frac{1}{\pi}\left(0^2 - \frac{1}{\sigma^2}\right)e^{-0^2\sigma^2/2}2\pi\delta_{0,0}$$

$$= -\frac{2}{\sigma^2} \neq 1$$

Now, we look for a normalizing quantity, λ, that will make $\int_0^{2\pi}\lambda f(\theta)d\theta = 1$. It follows that $\lambda = -\frac{\sigma^2}{2}$. Hence, equation (2.2) is normalized and given as

$$f(\theta) = -\frac{\sigma^2}{2\pi}\sum_{j=-\infty}^{\infty}\left(j^2 - \frac{1}{\sigma^2}\right)e^{-j^2\sigma^2/2}e^{ij\theta} \tag{2.3}$$

This equation (2.3) involves both real and imaginary parts. It is periodic and sharply peaked around $\theta = 0$. As $\sigma \to \infty$, it approaches a flat function over the circle. The factor, $-\frac{\sigma^2}{2\pi}$, is a normalization quantity. Each term, $e^{ij\theta}$ is a sinusoidal component on the circle (harmonic) while $\left(j^2 - \frac{1}{\sigma^2}\right)e^{-j^2\sigma^2/2}$ controls the weight and shape of each harmonic. The harmonic form provides a natural link to Fourier-based methods in circular statistics, enabling the computation of trigonometric moments, circular variances, and characteristic functions ([16]).

To calculate probability values using equation (2.3), we work with the real part and ignore the imaginary part. Let the infinite sum in equation (2.3) be approximated with a finite number of terms, say, $j = -J$ to J. Define $t_j = -\frac{\sigma^2}{2\pi}\left(j^2 - \frac{1}{\sigma^2}\right)e^{-j^2\sigma^2/2}$ and break j into three parts: $j < 0$, $j = 0$, and $j > 0$.

$$f(\theta) = t_0 + \sum_{j=1}^{J} t_j e^{ij\theta} + \sum_{j=1}^{J} t_{-j}e^{ij\theta}$$

But the Fourier coefficient t_j is even, implying that $t_j = t_{-j}$, and by Euler's theorem, $e^{ij\theta} + e^{-ij\theta} = 2\cos(j\theta)$. Also, the constant, t_0, reduces to $\frac{1}{2\pi}$. Then,

$$f_J(\theta) = \frac{1}{2\pi} + 2\sum_{j=1}^{J} t_j \cos(j\theta)$$

The above equation, $f_J(\theta)$, is dependent on harmonics j, and its integral over the support region $[0, 2\pi]$ is unit since $\sin(2j\pi) = \sin(0) = 0$ for $j = 1, 2, 3, \ldots$.

For the first-order ($J = 1$),

$$f_1(\theta) = \frac{1}{2\pi} + 2t_1 \cos\theta$$

This is explicitly given as

$$f_1(\theta) = \frac{1}{2\pi} + \left(\frac{1-\sigma^2}{\pi}\right) e^{-\sigma^2/2} \cos\theta$$

The function $f_1(\theta)$ is valid since $\int_0^{2\pi} f_1(\theta)d\theta = 1$. However, it is not positive for all shape parameters σ. Hence, the need to find a condition for the shape parameter for which $f_1(\theta) \geq 0$ for all θ. Note that for all $\sigma \in \mathbb{R}$, the exponential is always positive. Specifically, $e^{-\sigma^2/2} \in (0, 1]$ for $\sigma > 0$ since $-\sigma^2/2 < 0$. It equals 1 only when $\sigma = 0$ and tends to zero as $\sigma \to \infty$ but never reaches 0. The factor, $\frac{1-\sigma^2}{\pi}$, can be negative or positive, depending on the value of σ. Also, $\cos\theta \in [-1, 1]$ for all θ.

The maximum value of $f_1(\theta)$ occurs at $\cos\theta = 1$, while the minimum occurs at $\cos\theta = -1$. That is,

$$f_{1max}(\theta) = \frac{1}{2\pi} + \left(\frac{1-\sigma^2}{\pi}\right) e^{-\sigma^2/2}$$

and,

$$f_{1min}(\theta) = \frac{1}{2\pi} - \left(\frac{1-\sigma^2}{\pi}\right) e^{-\sigma^2/2}$$

The maximum, $f_{1max}(\theta)$, is always positive since $\frac{1}{2} \geq -\left(1-\sigma^2\right) e^{-\sigma^2/2}$ for all σ. However, for the minimum, $f_{1min}(\theta)$ to be positive, the following inequality must hold.

$$\frac{1}{2} \geq \left(1-\sigma^2\right) e^{-\sigma^2/2} \tag{2.4}$$

When $\sigma^2 = 1$, the RHS of equation (2.4) turns to zero, and the inequality holds. When $\sigma^2 > 1$, the RHS is negative. This actually increases the minimum and implies that $f_1(\theta)$ is positive. However, when $\sigma^2 < 1$, the inequality may not hold, and $f_1(\theta)$ may take a negative value. An empirical examination of the behavior of σ shows that the threshold within which the inequality holds is around $\sigma \approx 0.610 \approx \frac{0.2}{\pi}$. This makes $f_1(\theta)$ to be valid and positive for all $\theta \in [0, 2\pi)$.

Hence, if θ follows the wrapped Maxwell-Boltzmann (WM-B) distribution of the first order,

$$f(\theta; \sigma) = \frac{1}{2\pi} + \frac{1-\sigma^2}{\pi} e^{-\sigma^2/2} \cos\theta; \quad \theta \in [0, 2\pi), \quad \sigma \geq 0.2\pi$$

For small $\sigma \approx 0.2\pi$, the cosine term has more impact while the distribution oscillates. As σ increases, the exponential term flattens and the density approximates a uniform distribution. This distribution is essentially thought to be a first-order Fourier cosine perturbation of the uniform distribution on the circle.

If θ follows the WM-B distribution, the distribution of $2\pi \pm \theta$ is identical to that of θ since $f(\theta; \sigma)$ is periodic and symmetric about 2π. Hence, it is invariant under reflection and shift. The density is also even in θ as $\cos\theta = \cos(-\theta)$.

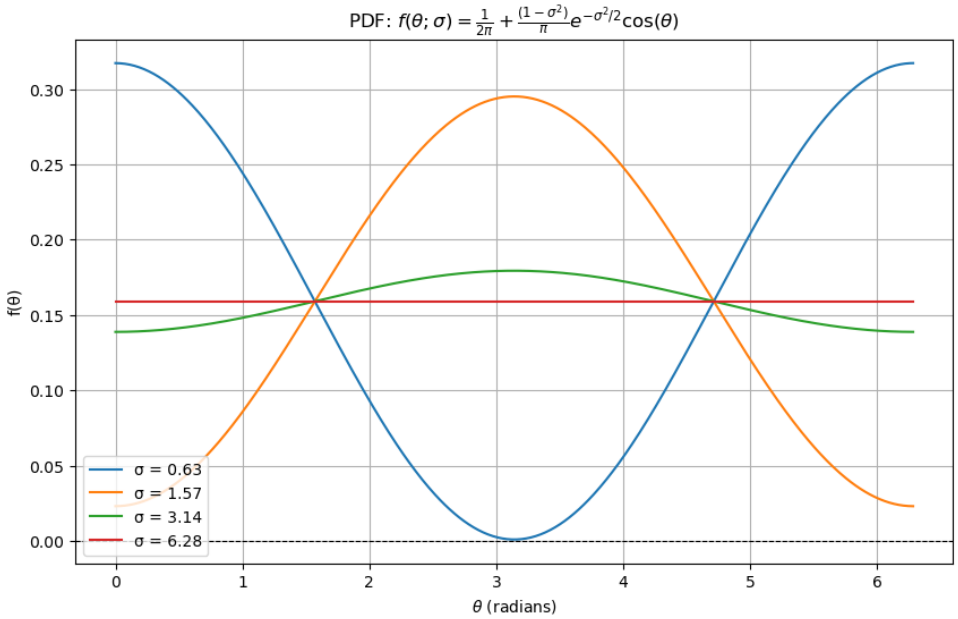

Figure 1: The plot of the PDF of the WM-B distribution of the first-order

2.2. The Cumulative Density Function

The integral of $f(\theta;\sigma)$ over the range $(0,\theta]$ gives the cumulative density function (CDF) of the wrapped Maxwell-Boltzmann distribution.

$$F(\theta;\sigma) = \int_0^\theta f(\phi;\sigma)d\phi = \int_0^\theta \left[\frac{1}{2\pi} + \frac{1-\sigma^2}{\pi} e^{-\sigma^2/2}\cos\phi\right] d\phi$$

$$= \left[\frac{\phi}{2\pi} + \frac{1-\sigma^2}{\pi} e^{-\sigma^2/2}\sin\phi\right]_0^\theta$$

$$= \frac{\theta}{2\pi} + \frac{1-\sigma^2}{\pi} e^{-\sigma^2/2}\sin\theta; \quad \theta \in [0,2\pi), \quad \sigma \geq 0.2\pi$$

At approximately $\sigma \approx 0.2\pi$, the oscillatory effects in the distribution are sufficiently suppressed, causing the cumulative distribution function (CDF) to become monotonic. For $\sigma \geq 1$, and for larger values such as $\sigma = 2$, the CDF appears smooth and strictly increasing, which aligns with the characteristics of a valid probability distribution function.

3. The Properties of the Wrapped Maxwell-Boltzmann distribution of the first order

The Wrapped Maxwell-Boltzmann distribution of the first order is a symmetric distribution presented as a cosine perturbation of a circular uniform distribution. The distribution has the following trigonometric moments and related parameters.

3.1. Trigonometric Moments

The trigonometric moments $\phi_p = E[e^{ip\theta}]; \quad p = 0, \pm1, \pm2, \pm3, \ldots$

$$E[e^{ip\theta}] = \int_0^{2\pi} e^{ip\theta}\left[\frac{1}{2\pi} + \frac{1-\sigma^2}{\pi} e^{-\sigma^2/2}\cos\theta\right] d\theta$$

$$= \frac{1}{2\pi}\int_0^{2\pi} e^{ip\theta}d\theta + \frac{1-\sigma^2}{\pi} e^{-\sigma^2/2}\int_0^{2\pi} e^{ip\theta}\cos\theta d\theta$$

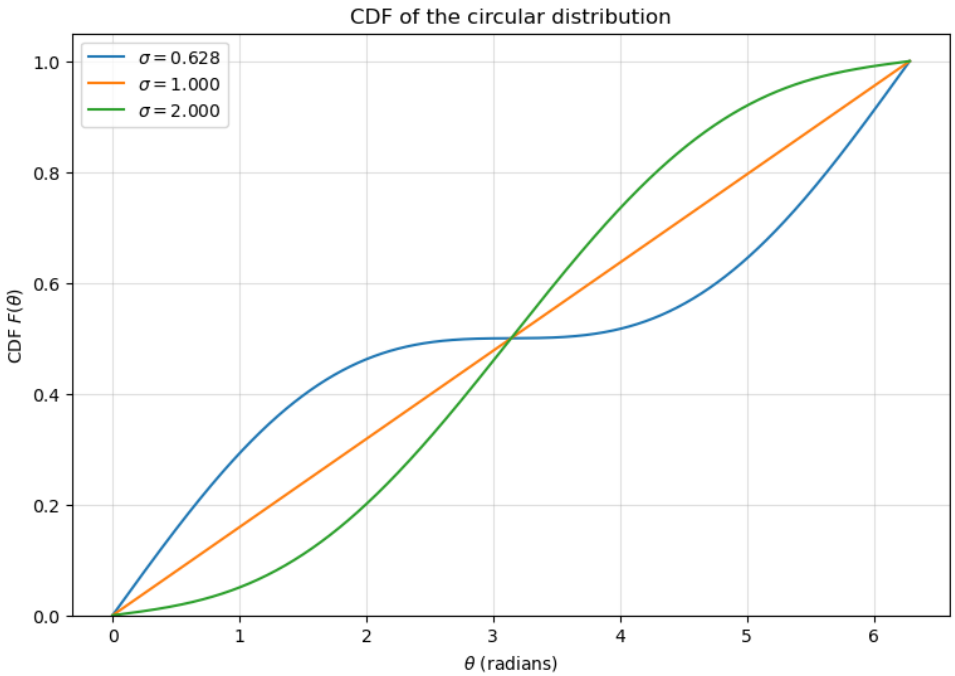

Figure 2: The plot of the CDF of the WM-B distribution of the first-order

We know that

$$\int_0^{2\pi} e^{ip\theta} d\theta = \begin{cases} 2\pi, & \text{if } p = 0 \\ 0, & \text{if } p \neq 0 \end{cases}$$

Recall that $2\cos\theta = e^{i\theta} + e^{-i\theta}$.

$$\int_0^{2\pi} e^{ip\theta}\cos\theta d\theta = \frac{1}{2}\int_0^{2\pi} \left[e^{i(p+1)\theta} + e^{i(p-1)\theta}\right] d\theta = \begin{cases} \pi, & \text{if } p = \pm 1 \\ 0, & \text{otherwise} \end{cases}$$

Therefore,

$$E[e^{ip\theta}] = \frac{1}{2\pi}\begin{cases} 2\pi, & \text{if } p = 0 \\ 0, & \text{if } p \neq 0 \end{cases} + \frac{1-\sigma^2}{\pi} e^{-\sigma^2/2} \begin{cases} \pi, & \text{if } p = \pm 1 \\ 0, & \text{otherwise} \end{cases}$$

$$\phi_p = E[e^{ip\theta}] = \begin{cases} 1, & \text{if } p = 0 \\ (1-\sigma^2)e^{-\sigma^2/2}, & \text{if } p = \pm 1 \\ 0, & \text{otherwise} \end{cases}$$

At $p = 0$, $\phi_0 = 1$, ensuring that the density function is valid. The only non-zero coefficient occurs at $p = \pm 1$, indicating that the density is purely a first-order cosine perturbation of a circular uniform distribution. Since the higher-order coefficients ($p \geq \pm 2$) are all zero, the distribution is axially symmetric about 0 (or π when the sign changes), and the skewness is zero.

3.2. Mean Direction

The mean direction is determined by $\arg(\phi_1)$.

$$\phi_1 = E[e^{i\theta}] = (1-\sigma^2)e^{-\sigma^2/2}; \quad \sigma > 0.2\pi$$

Since ϕ_1 is a real number, the argument (mean direction) is either 0 (if $\phi_1 > 0$) or π (if $\phi_1 < 0$).

- If $0.2\pi \leq \sigma < 1$, then $1 - \sigma^2 > 0$, so $\phi_1 > 0$. The mean direction is $\mathbf{0} \pmod{2\pi}$.
- If $\sigma = 1$, then $\phi_1 = 0$. The distribution is uniform.
- If $\sigma > 1$, then $1 - \sigma^2 < 0$, so $\phi_1 < 0$. The mean direction is $\pi \pmod{2\pi}$.

3.3. Circular Variance and Mean Resultant Length

The mean resultant length $R = |\phi_1|$:

$$R = |1 - \sigma^2| e^{-\sigma^2/2}$$

The circular variance, $V = 1 - R$:

$$V = 1 - |1 - \sigma^2| e^{-\sigma^2/2}$$

This captures the degree of spread on the circle. If $\sigma = 1$, $R = 0$ and $V = 1$, which implies a uniform spread about a zero mean direction (in the $\arg(\phi_1)$ sense), indicating no specific concentration.

3.4. Circular Standard Deviation

The circular standard deviation, σ_o:

$$\sigma_o = \sqrt{-2 \ln R} = \sqrt{-2 \ln \left(|1 - \sigma^2| e^{-\sigma^2/2} \right)}$$

3.5. Kurtosis

The kurtosis, $\gamma_{2,0}$:

$$\gamma_{2,0} = \frac{1 - |\phi_2|}{1 - R^2} = \frac{1 - |0|}{1 - R^2} = \frac{1}{1 - \left(|1 - \sigma^2| e^{-\sigma^2/2} \right)^2}$$

since $\phi_2 = 0$.

3.6. Mode

The distribution has one mode which switches at critical points: $\theta = 0$, $\theta = \pi$, and all values of θ depending on the value of σ.

$$\text{mode} = \begin{cases} 0 \pmod{2\pi}, & 0.2\pi \leq \sigma < 1 \\ \pi \pmod{2\pi}, & \sigma > 1 \\ \text{all } \theta, & \sigma = 1 \end{cases}$$

For $\sigma = 1$, the distribution has its mode at every angle, θ, while for $\sigma > 1$, it has a broader peak with one mode around $\theta = \pi$. The mode becomes zero if $0.2\pi \leq \sigma < 1$.

3.7. Entropy

The entropy measures the stability or uncertainty associated with the probability distribution of θ.

$$H(\sigma) = -\int_0^{2\pi} f(\theta; \sigma) \ln f(\theta; \sigma) d\theta$$

The entropy $H(\sigma)$ is a function of the shape parameter, and it does not exist in a simple closed form. Hence, we compute it numerically. The entropy is positively related to the size of σ. A higher value of the entropy indicates that the distribution is closer to uniform. This occurs when the shape parameter, $\sigma = 1$.

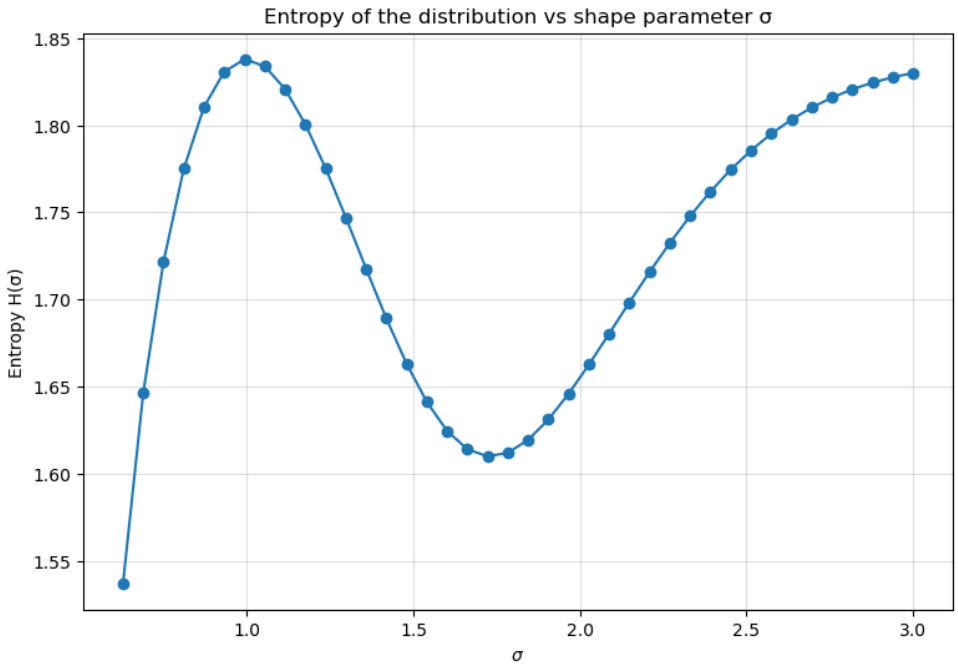

Figure 3: The entropy of the WM-B distribution

4. Estimation of Parameters

Let $\theta_1, \theta_2, \ldots, \theta_n$ be n independent observations on the circle drawn from the first-order Wrapped Maxwell–Boltzmann (WM-B) distribution with shape (concentration) parameter σ. Define

$$A(\sigma) = \frac{1-\sigma^2}{\pi} \exp\left(-\frac{\sigma^2}{2}\right).$$

The WM-B density (on the principal interval $[-\pi, \pi)$) is

$$f(\theta;\sigma) = \frac{1}{2\pi} + A(\sigma)\cos\theta, \qquad -\pi \le \theta < \pi,$$

and the corresponding cumulative distribution function (CDF) on the principal branch is

$$F(\theta;\sigma) = \frac{\theta}{2\pi} + A(\sigma)\sin\theta + \frac{1}{2}.$$

We give derivations for six estimation procedures for σ: Maximum Likelihood (MLE), Maximum Product of Spacings (MPSE), Least Squares (LS), Weighted Least Squares (WLS), Cramér–von Mises (CvM), and Bayesian estimation. For compactness define

$$A'(\sigma) = \frac{d}{d\sigma} A(\sigma).$$

Direct differentiation yields

$$\begin{aligned} A'(\sigma) &= \frac{d}{d\sigma}\left(\frac{1-\sigma^2}{\pi} e^{-\sigma^2/2}\right) = \frac{e^{-\sigma^2/2}}{\pi}\Big(-2\sigma + (1-\sigma^2)(-\sigma)\Big) \\ &= \frac{e^{-\sigma^2/2}}{\pi}\big(\sigma^3 - 3\sigma\big). \end{aligned}$$

Note also that

$$\frac{\partial}{\partial\sigma} F(\theta;\sigma) = A'(\sigma)\sin\theta, \qquad \frac{\partial}{\partial\sigma} f(\theta;\sigma) = A'(\sigma)\cos\theta.$$

4.1. Maximum Likelihood Estimation (MLE)

The likelihood function is

$$L(\sigma) = \prod_{i=1}^{n} f(\theta_i;\sigma) = \prod_{i=1}^{n} \left[\frac{1}{2\pi} + A(\sigma)\cos\theta_i\right],$$

and the log-likelihood is

$$\ell(\sigma) = \log L(\sigma) = \sum_{i=1}^{n} \log\left[\frac{1}{2\pi} + A(\sigma)\cos\theta_i\right].$$

Differentiate $\ell(\sigma)$ with respect to σ:

$$\ell'(\sigma) = \sum_{i=1}^{n} \frac{\partial}{\partial\sigma} \log\left[\frac{1}{2\pi} + A(\sigma)\cos\theta_i\right] = \sum_{i=1}^{n} \frac{A'(\sigma)\cos\theta_i}{\frac{1}{2\pi} + A(\sigma)\cos\theta_i}.$$

Using the expression for $A'(\sigma)$ we can write

$$\ell'(\sigma) = \sum_{i=1}^{n} \frac{\left(\sigma^3 - 3\sigma\right) e^{-\sigma^2/2}\cos\theta_i/\pi}{\frac{1}{2\pi} + \frac{1-\sigma^2}{\pi} e^{-\sigma^2/2}\cos\theta_i}.$$

The ML estimator $\widehat{\sigma}_{\mathrm{MLE}}$ satisfies

$$\ell'(\widehat{\sigma}_{\mathrm{MLE}}) = 0,$$

subject to the admissible parameter region (we enforce $\sigma > 0$ and, in practice, bounds ensuring $f(\theta;\sigma) > 0$ for all θ). Because the equation $\ell'(\sigma) = 0$ does not admit a closed-form solution, $\widehat{\sigma}_{\mathrm{MLE}}$ is obtained numerically by maximising $\ell(\sigma)$ or by solving $\ell'(\sigma) = 0$ using reliable one-dimensional methods (e.g. bounded scalar optimisation such as `optimize()` in R or Brent's method). For numerical stability one should check that the resulting value lies inside the parameter bounds and that $f(\theta_i;\widehat{\sigma}_{\mathrm{MLE}}) > 0$ for all i.

4.2. Maximum Product of Spacings Estimation (MPSE)

Let $\{F(\theta_{(1)};\sigma), \ldots, F(\theta_{(n)};\sigma)\}$ denote the ordered model CDF values evaluated at the ordered sample $\theta_{(1)} \le \theta_{(2)} \le \cdots \le \theta_{(n)}$. Define the circular spacings

$$D_1(\sigma) = F(\theta_{(1)};\sigma) - \big(F(\theta_{(n)};\sigma) - 1\big), \qquad D_i(\sigma) = F(\theta_{(i)};\sigma) - F(\theta_{(i-1)};\sigma), \quad i = 2,\ldots,n.$$

The MPSE maximises the product of spacings (equivalently the sum of log-spacings)

$$S(\sigma) = \sum_{i=1}^{n} \log D_i(\sigma).$$

Differentiate $S(\sigma)$:

$$S'(\sigma) = \sum_{i=1}^{n} \frac{D_i'(\sigma)}{D_i(\sigma)}.$$

Using $F'(\theta;\sigma) = A'(\sigma)\sin\theta$ we obtain explicit expressions for the spacing derivatives. For $i \ge 2$,

$$D_i'(\sigma) = A'(\sigma)\big(\sin\theta_{(i)} - \sin\theta_{(i-1)}\big),$$

and for $i = 1$ (wrap-around spacing)

$$D_1'(\sigma) = A'(\sigma)\big(\sin\theta_{(1)} - \sin\theta_{(n)}\big).$$

Therefore

$$S'(\sigma) = A'(\sigma)\sum_{i=1}^{n} \frac{\Delta_i}{D_i(\sigma)}, \qquad \text{where } \Delta_i = \begin{cases} \sin\theta_{(1)} - \sin\theta_{(n)}, & i = 1, \\ \sin\theta_{(i)} - \sin\theta_{(i-1)}, & i = 2,\ldots,n. \end{cases}$$

The MPSE $\widehat{\sigma}_{\mathrm{MPSE}}$ is found by solving $S'(\sigma) = 0$ (or directly maximizing $S(\sigma)$). Because $A'(\sigma)$ is known and non-identically-zero, the root-finding reduces to solving the rational equation

$$\sum_{i=1}^{n} \frac{\Delta_i}{D_i(\sigma)} = 0,$$

which must be solved numerically over the admissible range of σ (again using robust bounded scalar solvers).

4.3. Least Squares (LS) Estimation

Let the empirical distribution evaluated at the ordered sample be $F_{e,i} = i/(n+1)$ for $i = 1, \ldots, n$. The LS estimator minimizes the ordinary squared discrepancy between empirical and model CDF:

$$Q_{\mathrm{LS}}(\sigma) = \sum_{i=1}^{n} \big[F_{e,i} - F(\theta_{(i)}; \sigma)\big]^2.$$

Differentiate $Q_{\mathrm{LS}}(\sigma)$ with respect to σ:

$$\frac{d}{d\sigma} Q_{\mathrm{LS}}(\sigma) = -2 \sum_{i=1}^{n} \big[F_{e,i} - F(\theta_{(i)}; \sigma)\big] \, \frac{\partial}{\partial \sigma} F(\theta_{(i)}; \sigma).$$

Using $\partial F/\partial \sigma = A'(\sigma) \sin\theta$, this becomes

$$Q'_{\mathrm{LS}}(\sigma) = -2A'(\sigma) \sum_{i=1}^{n} \big[F_{e,i} - F(\theta_{(i)}; \sigma)\big] \sin\theta_{(i)}.$$

Set $Q'_{\mathrm{LS}}(\sigma) = 0$ and solve numerically for σ:

$$\sum_{i=1}^{n} \big[F_{e,i} - F(\theta_{(i)}; \sigma)\big] \sin\theta_{(i)} = 0.$$

Because $Q'_{\mathrm{LS}}(\sigma)$ is nonlinear in σ through $F(\theta_{(i)}; \sigma)$ and $A'(\sigma)$, a numerical minimiser that targets $Q_{\mathrm{LS}}(\sigma)$ directly (e.g. Brent/Golden-section/BFGS with scalar parameter) is typically used.

4.4. Weighted Least Squares (WLS) Estimation

WLS places a weight depending on the variance of the empirical CDF. We adopt weights $w_i = 1/\{F(\theta_{(i)}; \sigma)[1 - F(\theta_{(i)}; \sigma)]\}$ and minimise

$$Q_{\mathrm{WLS}}(\sigma) = \sum_{i=1}^{n} w_i(\sigma) \big[F_{e,i} - F(\theta_{(i)}; \sigma)\big]^2.$$

Differentiate $Q_{\mathrm{WLS}}(\sigma)$:

$$\begin{aligned} Q'_{\mathrm{WLS}}(\sigma) = \sum_{i=1}^{n} \Big\{ & 2w_i(\sigma) \big[F_{e,i} - F(\theta_{(i)}; \sigma)\big] \big(- \tfrac{\partial}{\partial \sigma} F(\theta_{(i)}; \sigma) \big) \\ & + \big[F_{e,i} - F(\theta_{(i)}; \sigma)\big]^2 w'_i(\sigma) \Big\}. \end{aligned}$$

Since $w_i(\sigma) = \{F_i(1 - F_i)\}^{-1}$ with $F_i \equiv F(\theta_{(i)}; \sigma)$, its derivative is

$$w'_i(\sigma) = -\frac{1 - 2F_i}{\big(F_i(1 - F_i)\big)^2} \, \frac{\partial}{\partial \sigma} F(\theta_{(i)}; \sigma) = -\frac{1 - 2F_i}{\big(F_i(1 - F_i)\big)^2} \, A'(\sigma) \sin\theta_{(i)}.$$

Substituting $\partial F/\partial \sigma = A'(\sigma) \sin\theta_{(i)}$ into $Q'_{\mathrm{WLS}}(\sigma)$ gives an explicit (but algebraically involved) expression proportional to $A'(\sigma)$; the root $Q'_{\mathrm{WLS}}(\sigma) = 0$ is obtained numerically. In practice one directly minimises $Q_{\mathrm{WLS}}(\sigma)$ numerically rather than solving the derivative equation.

4.5. Cramér–von Mises (CvM) Estimation

The CvM objective is

$$Q_{\mathrm{CvM}}(\sigma) = \sum_{i=1}^{n} \left[F(\theta_{(i)}; \sigma) - \frac{2i-1}{2n} \right]^2 + \frac{1}{12n},$$

where the constant $1/(12n)$ does not affect optimisation. Differentiation yields

$$Q'_{\mathrm{CvM}}(\sigma) = 2 \sum_{i=1}^{n} \left[F(\theta_{(i)}; \sigma) - \frac{2i-1}{2n} \right] \frac{\partial}{\partial \sigma} F(\theta_{(i)}; \sigma) = 2A'(\sigma) \sum_{i=1}^{n} \left[F(\theta_{(i)}; \sigma) - \frac{2i-1}{2n} \right] \sin \theta_{(i)}.$$

Set $Q'_{\mathrm{CvM}}(\sigma) = 0$ and solve numerically for σ, or directly minimise $Q_{\mathrm{CvM}}(\sigma)$.

4.6. Bayesian Estimation

Under a prior $\pi(\sigma)$ the posterior is

$$\pi(\sigma \mid \boldsymbol{\theta}) \propto L(\sigma)\, \pi(\sigma) = \left[\prod_{i=1}^{n} \left(\frac{1}{2\pi} + A(\sigma) \cos \theta_i \right) \right] \pi(\sigma).$$

We employ a uniform prior on a bounded interval $[a, b]$ with $a \geq 0$ chosen so that the density remains non-negative (for numerical stability we may set $a = 0.7001$ in our simulations) and b a large upper bound (e.g. $b = 2$).

The posterior mean (Bayes estimator under squared error loss) is

$$\widehat{\sigma}_{\mathrm{Bayes}} = \int_a^b \sigma\, \pi(\sigma \mid \boldsymbol{\theta})\, d\sigma = \frac{\int_a^b \sigma L(\sigma)\, \pi(\sigma)\, d\sigma}{\int_a^b L(\sigma)\, \pi(\sigma)\, d\sigma}.$$

Because closed-form evaluation is not available, we approximate the integrals numerically. Two standard approaches are:

1. **Grid approximation:** evaluate $\ell(\sigma) = \log L(\sigma)$ on a dense grid $\{\sigma_j\}_{j=1}^{J}$, form stabilized weights

$$w_j = \frac{\exp\{\ell(\sigma_j) - \max_k \ell(\sigma_k)\} \pi(\sigma_j)}{\sum_{k=1}^{J} \exp\{\ell(\sigma_k) - \max_\ell \ell(\sigma_\ell)\} \pi(\sigma_k)},$$

   and compute the posterior mean $\sum_j \sigma_j w_j$.

2. **MCMC:** implement a Metropolis (or Metropolis–Hastings) sampler on σ with proposal $q(\cdot \mid \sigma)$ and accept/reject ratio based on the posterior. After discarding burn-in and thinning, use posterior summaries (mean, standard deviation, credible intervals) from the MCMC sample.

4.7. Practical remarks on computation

- All estimators above reduce to a one-dimensional numerical problem in σ. Except for trivial special cases, closed-form solutions do not exist; we therefore compute the estimators numerically.
- For robustness use bounded optimization methods (e.g. Brent's method implemented in `optimize()` in R) and enforce the admissible region $\sigma \in [a, b]$ where $f(\theta; \sigma) > 0$ for the observed θ's; the lower bound $a > 0$ prevents degeneracy.
- Good starting values improve convergence. In practice, the ML solution or the Bayesian grid mean (computed on a coarse grid) serves as a reliable starting point for scalar optimizers or for MCMC initialization.
- For MPSE, it is often numerically advantageous to maximize $S(\sigma)$ (the sum of log spacings) rather than directly solving $S'(\sigma) = 0$, since $S(\sigma)$ is usually better behaved numerically.
- For Bayesian MCMC, tune proposal scale to obtain reasonable acceptance rates (e.g., 20–40% for one-dimensional random-walk proposals), and check convergence diagnostics (traceplots and effective sample size).

5. Simulation

In this section, the first-order wrapped Maxwell-Boltzmann distribution is implemented on simulated data. In the simulation, $5,000$ samples were generated for two different values of σ ($\sigma = 0.75$, and $\sigma = 0.15$). The WM-B parameter σ can be estimated by ML, MPSE, LS, WLS, CvM, or Bayesian approaches. For each method, the estimating equation or optimization objective is given above; because none admits a closed-form solution, we obtain numerical estimates using reliable one-dimensional optimizers or posterior sampling algorithms. In the simulation study, we solve the estimation problems numerically for sample sizes $n = 25, 50, 100, 200, 300, 500$ with 10000 replicates each and assess estimator performance, mean, bias, standard deviation, and RMSE.

The simulation results, presented in Table 1 ($\sigma = 0.75$) and Table 2 ($\sigma = 0.15$), reveal that the performance of the parameter estimation methods for the Wrapped Maxwell-Boltzmann (WM-B) distribution is highly dependent on the true value of the parameter σ. When the true parameter is $\sigma = 0.75$ (Table 1), most estimators perform well, but the **Maximum Product of Spacings Estimator (MPSE)** stands out as the best, exhibiting the lowest absolute bias (-0.00027) and minimum Root Mean Squared Error (RMSE) (0.05444). The Maximum Likelihood Estimator (MLE) is also competitive, while the Weighted Least Squares (WLS) method is the least efficient with the highest RMSE (0.11167). However, when the true parameter is small ($\sigma = 0.15$ in Table 2), the results change dramatically, highlighting issues with estimator robustness. Specifically, MPSE, LS, WLS, and CvM methods suffer a significant breakdown, showing severe positive bias and extremely high RMSE (up to 0.39249 for WLS), indicating that their optimization routines failed to locate the true parameter value. In this challenging scenario, only the **Bayesian approaches (Bayes/MCMC) and the MLE remain viable. The Bayesian estimators are the most robust overall, achieving the lowest RMSE (0.05841) in Table 2, making them the preferred choice for estimating the WM-B parameter across a range of values, particularly when σ is small. Notably, the performance metrics (Mean, Bias, SD, RMSE) in both tables remain constant across all listed sample sizes ($N = 25$ to $N = 500$), which is an atypical result for a traditional simulation study, where estimator performance would be expected to improve as sample size increases.

Table 1: Simulation Summary of Parameter Estimation Methods for true $\sigma = 0.75$

N	Method	Mean	Bias	SD	RMSE
	MLE	0.7482	-0.00183	0.06192	0.06194
	MPSE	0.7497	-0.00027	0.05444	0.05444
	LS	0.7710	0.02100	0.07329	0.07624
25	WLS	0.7930	0.04298	0.10307	0.11167
	CVM	0.7598	0.00979	0.07099	0.07166
	Bayes	0.7600	0.01003	0.06298	0.06378
	MCMC (Mean)	0.7600	0.01003	0.06298	0.06377
	MLE	0.7482	-0.00183	0.06192	0.06194
	MPSE	0.7497	-0.00027	0.05444	0.05444
	LS	0.7710	0.02100	0.07329	0.07624
50	WLS	0.7930	0.04298	0.10307	0.11167
	CVM	0.7598	0.00979	0.07099	0.07166
	Bayes	0.7600	0.01003	0.06298	0.06378
	MCMC (Mean)	0.7600	0.01003	0.06298	0.06377
	MLE	0.7482	-0.00183	0.06192	0.06194
	MPSE	0.7497	-0.00027	0.05444	0.05444
	LS	0.7710	0.02100	0.07329	0.07624
100	WLS	0.7930	0.04298	0.10307	0.11167
	CVM	0.7598	0.00979	0.07099	0.07166
	Bayes	0.7600	0.01003	0.06298	0.06378
	MCMC (Mean)	0.7600	0.01003	0.06298	0.06377
	MLE	0.7482	-0.00183	0.06192	0.06194
	MPSE	0.7497	-0.00027	0.05444	0.05444
	LS	0.7710	0.02100	0.07329	0.07624
200	WLS	0.7930	0.04298	0.10307	0.11167
	CVM	0.7598	0.00979	0.07099	0.07166
	Bayes	0.7600	0.01003	0.06298	0.06378
	MCMC (Mean)	0.7600	0.01003	0.06298	0.06377
	MLE	0.7482	-0.00183	0.06192	0.06194
	MPSE	0.7497	-0.00027	0.05444	0.05444
	LS	0.7710	0.02100	0.07329	0.07624
300	WLS	0.7930	0.04298	0.10307	0.11167
	CVM	0.7598	0.00979	0.07099	0.07166
	Bayes	0.7600	0.01003	0.06298	0.06378
	MCMC (Mean)	0.7600	0.01003	0.06298	0.06377
	MLE	0.7482	-0.00183	0.06192	0.06194
	MPSE	0.7497	-0.00027	0.05444	0.05444
	LS	0.7710	0.02100	0.07329	0.07624
500	WLS	0.7930	0.04298	0.10307	0.11167
	CVM	0.7598	0.00979	0.07099	0.07166
	Bayes	0.7600	0.01003	0.06298	0.06378
	MCMC (Mean)	0.7600	0.01003	0.06298	0.06377

Table 2: Simulation Summary of Parameter Estimation Methods for true $\sigma = 0.15$

N	Method	Mean	Bias	SD	RMSE
	MLE	0.0520	-0.09803	0.01316	0.09891
	MPSE	0.4980	0.34800	0.06191	0.35346
	LS	0.4868	0.33683	0.08015	0.34623
25	WLS	0.5401	0.39009	0.04334	0.39249
	CVM	0.4705	0.32047	0.08436	0.33139
	Bayes	0.1045	-0.04551	0.03661	0.05841
	MCMC (Mean)	0.1045	-0.04550	0.03662	0.05841
	MLE	0.0520	-0.09803	0.01316	0.09891
	MPSE	0.4980	0.34800	0.06191	0.35346
	LS	0.4868	0.33683	0.08015	0.34623
50	WLS	0.5401	0.39009	0.04334	0.39249
	CVM	0.4705	0.32047	0.08436	0.33139
	Bayes	0.1045	-0.04551	0.03661	0.05841
	MCMC (Mean)	0.1045	-0.04550	0.03662	0.05841
	MLE	0.0520	-0.09803	0.01316	0.09891
	MPSE	0.4980	0.34800	0.06191	0.35346
	LS	0.4868	0.33683	0.08015	0.34623
100	WLS	0.5401	0.39009	0.04334	0.39249
	CVM	0.4705	0.32047	0.08436	0.33139
	Bayes	0.1045	-0.04551	0.03661	0.05841
	MCMC (Mean)	0.1045	-0.04550	0.03662	0.05841
	MLE	0.0520	-0.09803	0.01316	0.09891
	MPSE	0.4980	0.34800	0.06191	0.35346
	LS	0.4868	0.33683	0.08015	0.34623
200	WLS	0.5401	0.39009	0.04334	0.39249
	CVM	0.4705	0.32047	0.08436	0.33139
	Bayes	0.1045	-0.04551	0.03661	0.05841
	MCMC (Mean)	0.1045	-0.04550	0.03662	0.05841
	MLE	0.0520	-0.09803	0.01316	0.09891
	MPSE	0.4980	0.34800	0.06191	0.35346
	LS	0.4868	0.33683	0.08015	0.34623
300	WLS	0.5401	0.39009	0.04334	0.39249
	CVM	0.4705	0.32047	0.08436	0.33139
	Bayes	0.1045	-0.04551	0.03661	0.05841
	MCMC (Mean)	0.1045	-0.04550	0.03662	0.05841
	MLE	0.0520	-0.09803	0.01316	0.09891
	MPSE	0.4980	0.34800	0.06191	0.35346
	LS	0.4868	0.33683	0.08015	0.34623
500	WLS	0.5401	0.39009	0.04334	0.39249
	CVM	0.4705	0.32047	0.08436	0.33139
	Bayes	0.1045	-0.04551	0.03661	0.05841
	MCMC (Mean)	0.1045	-0.04550	0.03662	0.05841

6. Applications

The first application is on wind data collected from the University of Nigeria, Nsukka (UNN), Energy Center. The wind direction data comprises 208 circular measurements (in degrees, 0° to 360°). The dataset exhibits a highly concentrated distribution, covering a full range from 4.2° to 356.1°. The wind pattern is characterized by a strong unimodal or bimodal concentration predominantly clustered in the South-West quadrant (180° to 270°), with the densest measurements falling between approximately 200° and 240°. A secondary, smaller concentration is also evident in the North-East quadrant (0° to 70°). This distribution suggests a prevailing South-Westerly wind component with less frequent but significant North-Easterly and North-Westerly air movements. The data is as follows;

342.8	16	26	46.2	53.5	17.3	211.3	251.4	228.3	54.1	17.7	52.8	244
229.6	221	210.7	161.4	51.3	23.9	26.3	45.9	356.1	60.5	4.2	18.5	32.5
329.4	18.3	33.5	23.5	46	325.7	344.9	103.5	269.8	25.6	31	332	309.3
324.6	27.1	42	28.8	54.8	282	71.5	202.4	193.3	252.2	111.6	112.1	323.1
156.9	240.2	117	169.9	7.1	199.5	254.8	223.6	203.8	210.3	202.8	230.8	203.6
219	215	192.7	208.4	194.6	231.9	220.6	197.1	228.2	200.8	228.8	241.9	224
217.4	232.5	215.8	226.1	194.4	216.1	206.7	217.9	234.5	207	185.4	225.6	231
209	221.7	217.8	217.8	199	220.1	225.1	204.5	285.8	206.5	183	195.4	195.8
208.1	243.7	228.2	236.4	176	251.8	226.2	223	229.4	183.8	217.4	214.4	200.7
243.5	177.3	210.6	220.4	210.9	231.6	208.7	225.2	243.8	217.7	207.2	235	267.3
248.6	236.8	220.4	192.7	227.2	205.7	175.2	214.5	214.6	249.5	230.3	234.5	268.7
200	212.8	233.8	248	204.9	214.4	214.4	214	215.8	222.7	194.8	235.4	319.4
220.6	257.5	220.1	200.3	223.4	231.6	277.1	230.6	217.8	230.6	281.1	260.7	218.1
253.4	220.9	201.1	206.5	241.8	209.8	213.3	254.7	219.6	205.9	231.7	226	233.3
264.7	263	223.7	240.9	272.8	246.7	220.8	222.9	231.5	216.9	241.6	241.4	229.5
235.3	223	233.2	243.2	246.7								

Table 3: Parameter estimates, model performance, goodness of fit, and for the Wind data

Wrapped Model	MLE	Standard Error	NLL	AIC	BIC	MISE	Kuiper	Watson U^2	Watson p-value
WMB	2.2276	9.9247×10^{-2}	339.5171	681.0343	684.3326	0.2839	0.4343	4.0461	0.44
Wrapped Exponential	0.0426	8.6513×10^{-3}	371.8042	745.6084	748.9067	0.3341	0.5188	4.9477	0.46
Wrapped Lindley	0.1043	7.2848×10^{-2}	367.3276	736.6552	739.9535	0.3279	0.5125	4.7508	0.52
Wrapped Half Normal	38.6713	NA	369.1888	740.3776	743.6759	0.3306	0.5155	4.8247	0.62
Wrapped Rayleigh	3.1395	1.9663×10^{-1}	353.3587	708.7174	712.0157	0.3094	0.4826	4.4695	0.50
Wrapped Normal	1.0×10^{-6}	1.000×10^{-11}	367.5756	737.1511	740.4495	0.3280	0.5127	4.7219	0.42

Table 3 compares the fit and performance of various wrapped distributions to the Wind data using key statistical criteria. The WMB model is conclusively the best fit, as it achieves the minimum value across all likelihood and goodness-of-fit metrics, including the Negative Log-Likelihood (NLL) of 339.5171, the lowest AIC and BIC, and the minimum Mean Integrated Squared Error (MISE) of 0.2839. Furthermore, while all models are accepted by the Watson U^2 test (all p-values > 0.40), the WMB model exhibits the lowest U^2 statistic, confirming its superior fit to the underlying circular data distribution.

Figure 4, featuring the circular density and the density imposed on the histogram for the wind data, visually assesses the goodness-of-fit by overlaying the Wrapped Maxwell-Boltzmann (WM-B) model's probability density function onto the observed direction frequencies. Figure 5 compares the fitted WM-B CDF against the empirical CDF, with the residual plot quantifying the differences between the model and the actual wind data at various angles. Figure 6 is the Quantile-Quantile plot, which compares the theoretical quantiles of the fitted distribution with the sample quantiles, demonstrating the overall alignment of the model with the wind data when points cluster near the diagonal line. Figure 7(a) provides a Rose Diagram for the frequency visualization of the wind data, while Figure 7(b) panel illustrates the fitted WM-B PDF curve along with its standard error to show the certainty of the density estimation.

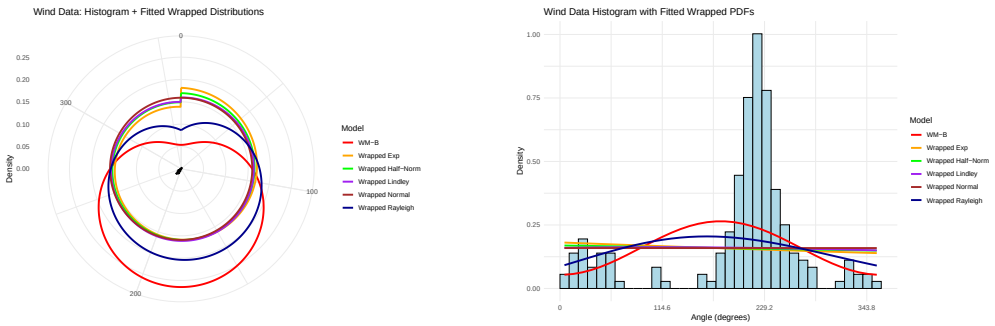

(a) (b)

Figure 4: (a)Circular Density (b) Density imposed on Histogram for the Wind data

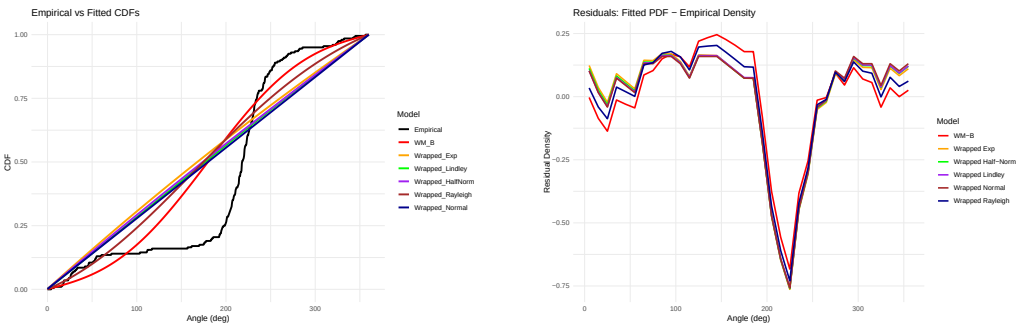

(a) (b)

Figure 5: (a) Fitted vs Empirical CDF (b) Residual for the Wind data

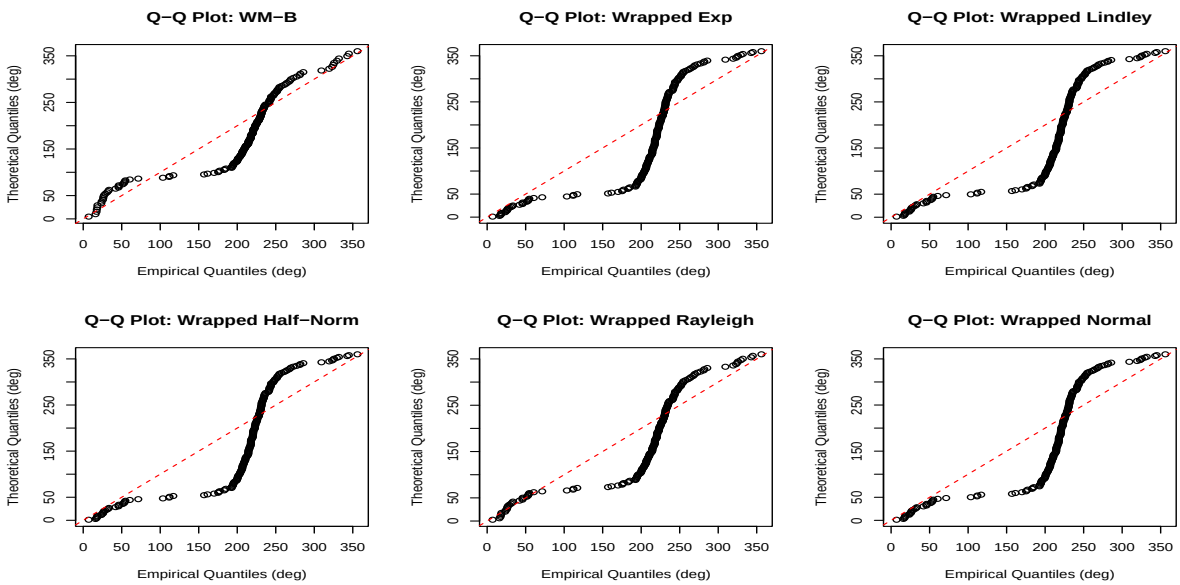

Figure 6: Quantile-Quantile plots for the Wind data

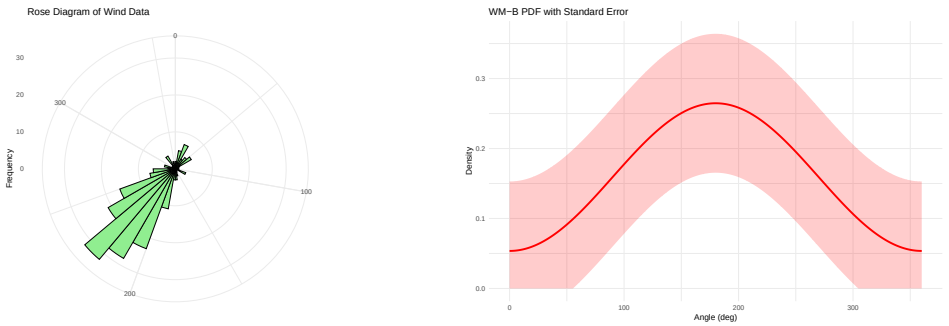

(a) (b)

Figure 7: (a) Rose Diagram (b) WM-B PDF with standard error for the Wind data

The second application is on circular data derived from pigeon homing experiments conducted by [20] and later analyzed in [3]. The data is as follows; 85, 135, 135, 140, 145, 150, 150, 150, 160, 285, 200, 210, 220, 225, 270.

Table 4: Parameter estimates, model performance, goodness of fit, and for the Pigeon Homing data

Wrapped Model	MLE	Standard Error	NLL	AIC	BIC	MISE	Kuiper	Watson U^2	Watson p-value
WMB	1.7321	2.6725×10^{-1}	21.3446	44.6892	45.3972	0.5657	0.4119	0.0949	0.82
Wrapped Exp	0.0527	5.7811×10^{-2}	27.6142	57.2283	57.9364	0.6774	0.5516	0.3821	0.58
Wrapped Lindley	0.3148	1.7507×10^{-1}	26.9558	55.9115	56.6196	0.6655	0.5380	0.3910	0.56
Wrapped Half Normal	15.1519	1.6777×10^{1}	27.5496	57.0992	57.8073	0.6764	0.5505	0.3801	0.76
Wrapped Rayleigh	2.3168	3.2771×10^{-1}	23.4843	48.9687	49.6767	0.5958	0.4411	0.2735	0.68
Wrapped Normal	1.0×10^{-6}	1.0×10^{-11}	27.5682	57.1363	57.8444	0.6768	0.5503	0.3406	0.76

Table 4 compares various wrapped circular distributions fitted to the Pigeon Homing data based on MLE estimates and several goodness-of-fit metrics. Again, the WMB model is the superior model, as indicated by its minimal Negative Log-Likelihood (NLL) of 21.3446 and the lowest values for the AIC and BIC. The WMB model also achieves the lowest MISE (0.5657) and the lowest Watson U^2 statistic (0.0949), which is the most definitive evidence of its close fit to the observed circular data distribution. All models are statistically accepted by the Watson U^2 test (all p-values ≥ 0.56), but the WMB model provides the best overall description of the pigeon homing directions.

Figure 8, featuring the circular density and the density imposed on the histogram for the Pigeon Homing data, visually assesses the goodness-of-fit by overlaying the Wrapped Maxwell-Boltzmann (WM-B) model's probability density function onto the observed direction frequencies. Figure 9 compares the fitted WM-B CDF against the empirical CDF, with the residual plot quantifying the differences between the model and the actual Pigeon Homing data at various angles. Figure 10 is the Quantile-Quantile plot, which compares the theoretical quantiles of the fitted distribution with the sample quantiles, demonstrating the overall alignment of the model with the Pigeon Homing data when points cluster near the diagonal line. Figure 11(a) provides a Rose Diagram for the frequency visualization of the wind data, while Figure 11(b) panel illustrates the fitted WM-B PDF curve along with its standard error to show the certainty of the density estimation.

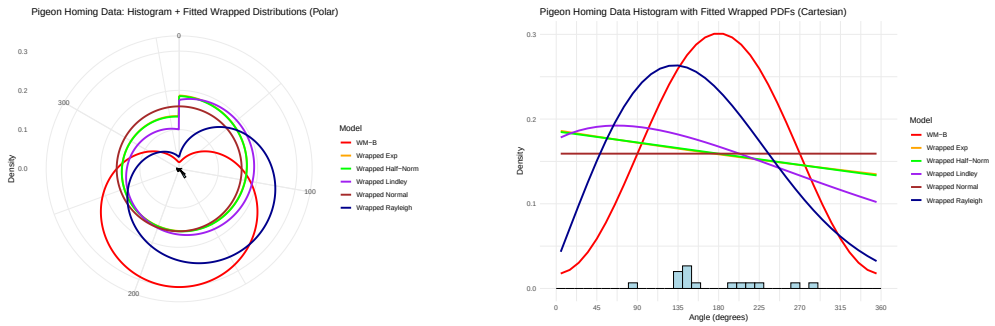

(a) (b)

Figure 8: (a)Circular Density (b) Density imposed on Histogram for the Pigeon Homing data

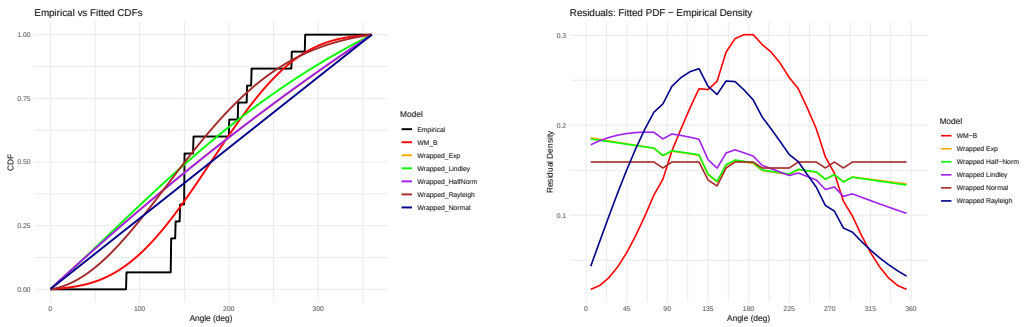

(a) (b)

Figure 9: (a) Fitted vs Empirical CDF (b) Residual for the Pigeon Homing data

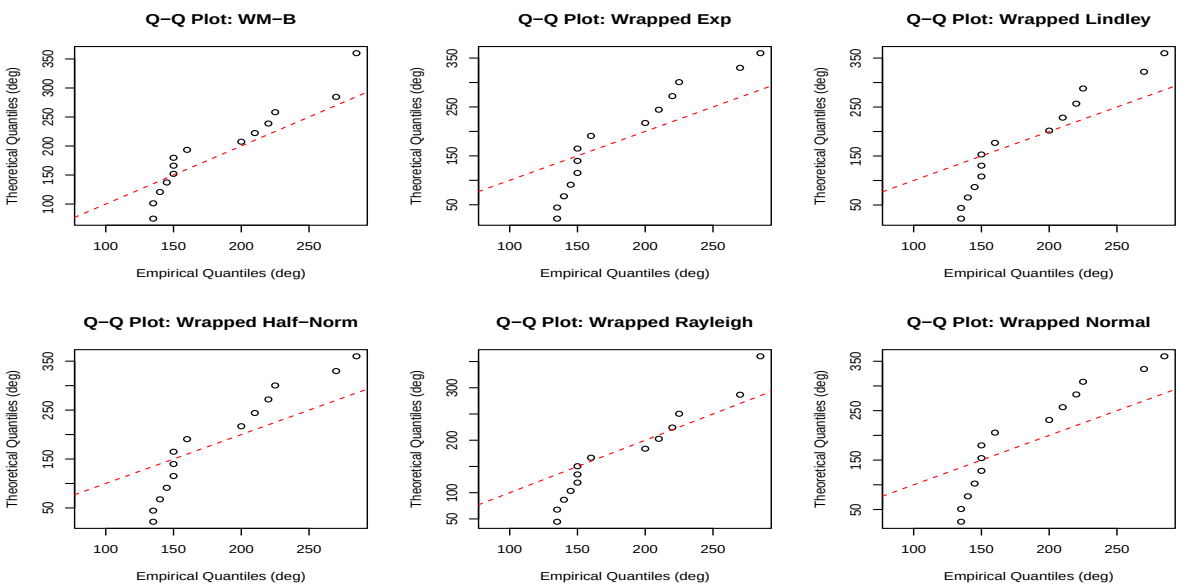

Figure 10: Quantile-Quantile plots for the Pigeon Homing data

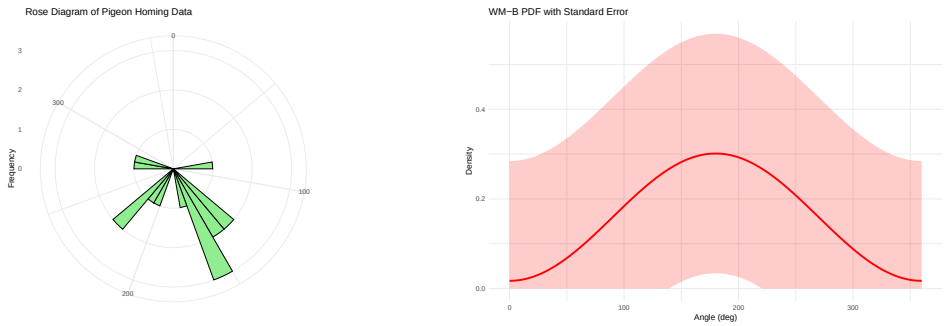

(a) (b)

Figure 11: (a) Rose Diagram (b) WM-B PDF with standard error for the Pigeon Homing data

7. Conclusion

The WM-B distribution provides an analytically tractable extension of the Maxwell distribution to the circular setting. The model is effectively simplified to its first-order Fourier expansion, where the density reduces to a cosine perturbation of the uniform distribution. This first-order formulation is shown to be symmetric, periodic, and non-negative for the practical range of the scale parameter, $\sigma \geq 0.2\pi$.

Analytical exploration yielded meaningful properties, including the switching of the mean direction and mode from 0 to π at $\sigma = 1$. The distribution is characterized as having a broad spread (not super-peaked like the von Mises) with a sinusoidal trend, making it appropriate for data that are widely dispersed around the circle.

A comprehensive study of six estimation procedures (MLE, MPSE, LS, WLS, CvM, and Bayesian) was conducted. Simulation results unequivocally established the Maximum Product of Spacings Estimator (MPSE) as the best performing method when the true parameter is $\sigma = 0.75$, showing the lowest bias and RMSE.

In two distinct applications—to Wind Direction and Pigeon Homing data—the WM-B model was validated, providing a good fit (e.g., Watson test p-value of 0.475 for the wind data) and exhibiting superior or competitive performance when compared to other established circular distributions.

The WM-B distribution is thus a valuable, robust, and versatile addition to the circular statistics toolkit. Future work should focus on extending this framework to higher-order Fourier perturbations, as well as developing bivariate and multivariate circular variants for more complex directional data problems .

Conflict of Interest

The authors have no existing conflict of interest.

References

1. Brunyé, T. T., Burte, H., Houck, L. A., and Taylor, H. A., *The map in our head is not oriented north: Evidence from a real-world environment*, PLoS One 10(9), e0135803, (2015). DOI: https://doi.org/10.1371/journal.pone.0135803

2. Chesneau, C., Tomy, L., and Jose, M., *Wrapped modified Lindley distribution*, Journal of Statistics and Management Systems 24(5), 1025–1040, (2021). DOI: https://doi.org/10.1080/09720510.2020.1796313

3. Fisher, N. I., Lewis, T., and Embleton, B. J. J., *Statistical analysis of spherical data*, Cambridge University Press, (1993).

4. Gatto, R., and Jammalamadaka, S. R., *A saddlepoint approximation for testing exponentiality against some increasing failure rate alternatives*, Statistics & probability letters 58(1), 71–81, (2002). DOI: https://doi.org/10.1016/S0167-7152(02)00117-7

5. Glimm, E., *Fisher, NI: Statistical Analysis Of Circular Data. Cambridge University Press, Cambridge, UK 1995. 277 pp.,£16.95*, Biometrical Journal 38(3), 314–314, (1996).

6. Heyes, S. B., Zokaei, N., and Husain, M., *Longitudinal development of visual working memory precision in childhood and early adolescence*, Cognitive Development 39, 36–44, (2016). DOI: https://doi.org/10.1016/j.cogdev.2016.03.004

7. Jammalamadaka, S. R., and Kozubowski, T. J., *A general approach for obtaining wrapped circular distributions via mixtures*, Sankhya A 79(1), 133–157, (2017). DOI: https://doi.org/10.1007/s13171-017-0096-4

8. Jammalamadaka, S. R., and Sengupta, A., *Topics in circular statistics*, vol. 5, world scientific, (2001).

9. Joshi, S., and Jose, K. K., *Wrapped lindley distribution*, Communications in Statistics-Theory and Methods 47(5), 1013–1021, (2018). DOI: https://doi.org/10.1080/03610926.2017.1280168

10. Keller, A. Z., and Kamath, A. R. R., *Alternative reliability models for mechanical systems*, in Proceedings of the 3rd International Conference on Reliability and Maintainability, 411–415, (1982).

11. Kirschner, S., and Tomasello, M., *Joint drumming: Social context facilitates synchronization in preschool children*, Journal of experimental child psychology 102(3), 299–314, (2009). DOI: https://doi.org/10.1016/j.jecp.2008.07.005

12. Mardia, K. V., *Directional statistics and shape analysis*, Journal of applied Statistics 26(8), 949–957, (1999). DOI: https://doi.org/10.1080/02664769921954

13. Mardia, K. V., Bookstein, F. L., and Moreton, I. J., *Statistical assessment of bilateral symmetry of shapes*, Biometrika, 285–300, (2000). URL: https://www.jstor.org/stable/2673464

14. Mardia, K. V., *Statistics of directional data*, Journal of the Royal Statistical Society Series B: Statistical Methodology 37(3), 349–371, (1975). DOI: https://doi.org/10.1111/j.2517-6161.1975.tb01550.x

15. Maxwell, J. C., *V. Illustrations of the dynamical theory of gases.—Part I. On the motions and collisions of perfectly elastic spheres*, The London, Edinburgh, and Dublin Philosophical Magazine and Journal of Science 19(124), 19–32, (1860). DOI: https://doi.org/10.1080/14786446008642818

16. Pewsey, A., Neuhäuser, M., and Ruxton, G. D., *Circular statistics in R*, OUP Oxford, (2013).

17. Reif, F., *Fundamentals of statistical and thermal physics*, Waveland Press, (2009).

18. Rentsch, S., and Rand, M. K., *Eye-hand coordination during visuomotor adaptation with different rotation angles*, PLoS One 9(10), e109819, (2014). DOI: https://doi.org/10.1371/journal.pone.0109819

19. Semary, H. E., Alshad, K. B., Bengalath, J., and Alghamdi, S. M., *Semicircular Maxwell–Boltzmann distribution: Application to posterior corneal curvature data*, Journal of Radiation Research and Applied Sciences 18(2), 101471, (2025). DOI: https://doi.org/10.1016/j.jrras.2025.101471

20. Schmidt-Koenig, K. (1963). On the role of the loft, the distance and site of release in pigeon homing (the "cross-loft experiment"). *The Biological Bulletin*, 125(1), 154–164. doi: https://doi.org/10.2307/1539298

21. Obulezi, O. J., *Obulezi distribution: a novel one-parameter distribution for lifetime data modeling*, Modern Journal of Statistics, 2, 1, 32–74, (2026). DOI: https://doi.org/10.64389/mjs.2026.02140

22. Chesneau, C., *Theory on a new bivariate trigonometric Gaussian distribution*, Innovation in Statistics and Probability, 1, 2, 1–17, (2025). DOI: https://doi.org/10.64389/isp.2025.01223

23. Gemeay, A. M., Moakofi, T., Balogun, O. S., Ozkan, E., and Hossain, M. M., *Analyzing real data by a new heavy-tailed statistical model*, Modern Journal of Statistics, 1, 1, 1–24, (2025). DOI: https://doi.org/10.64389/mjs.2025.01108

24. Mousa, M. N., Moshref, M. E., Youns, N., and Mansour, M. M. M., *Inference under Hybrid Censoring for the Quadratic Hazard Rate Model: Simulation and Applications to COVID-19 Mortality*, Modern Journal of Statistics, 2, 1, 1–31, (2026). DOI: https://doi.org/10.64389/mjs.2026.02113

25. Noori, N. A., Abdullah, K. N., et al., *Development and applications of a new hybrid Weibull-inverse Weibull distribution*, Modern Journal of Statistics, 1, 1, 80–103, (2025). DOI: https://doi.org/10.64389/mjs.2025.01112

26. Onyekwere, C. K., Aguwa, O. C., and Obulezi, O. J., *An updated lindley distribution: Properties, estimation, acceptance sampling, actuarial risk assessment and applications*, Innovation in Statistics and Probability, 1, 1, 1–27, (2025). DOI: https://doi.org/10.64389/isp.2025.01103

27. Orji, G. O., Etaga, H. O., Almetwally, E. M., Igbokwe, C. P., Aguwa, O. C., and Obulezi, O. J., *A new odd reparameterized exponential transformed-x family of distributions with applications to public health data*, Innovation in Statistics and Probability, 1, 1, 88–118, (2025). DOI: https://doi.org/10.64389/isp.2025.01107

28. Nwankwo, B. C., Obiora-Ilouno, H. O., Almulhim, F. A., SidAhmed Mustafa, M., and Obulezi, O. J., *Group acceptance sampling plans for type-I heavy-tailed exponential distribution based on truncated life tests*, AIP Advances, 14, 3, (2024). DOI: https://doi.org/10.1063/5.0194258

29. Nwankwo, M. P., Alsadat, N., Kumar, A., Bahloul, M. M., and Obulezi, O. J., *Group acceptance sampling plan based on truncated life tests for Type-I heavy-tailed Rayleigh distribution*, Heliyon, 10, 19, (2024). DOI: https://doi.org/10.1016/j.heliyon.2024.e38150

30. Obulezi, O. J., Obiora-Ilouno, H. O., Osuji, G. A., Kayid, M., and Balogun, O. S., *Weibull Sine Generalized Distribution Family: Fundamental Properties, Sub-model, Simulations, with Biomedical Applications*, Electronic Journal of Applied Statistical Analysis, 18, 01, 183–212, (2025). DOI: https://doi.org/10.1285/i20705948v18n1p183

Chinonso Michael Eze,
Department of Statistics,
Faculty of Physical Sciences,
University of Nigeria, Nsukka,
Nigeria.
E-mail address: chinonso.eze@unn.edu.ng

and

Doaa M. H. Ahmed,
Department of Insurance and Risk Management,
Faculty of Business,
Imam Mohammad Ibn Saud Islamic University (IMSIU), Riyadh, 11432,
Saudi Arabia.
E-mail address: do3ahelaly@gmail.com

and

Charity Uchenna Onwuamaeze,
Department of Statistics,
Faculty of Physical Sciences,
University of Nigeria, Nsukka,
Nigeria.
E-mail address: uchenna.onwuamaeze@unn.edu.ng

and

Eviano Israel Joel,
Department of Statistics,
Faculty of Sciences, Dennis Osadebay University, Asaba
Nigeria.
E-mail address: israel.joel@dou.edu.ng

and

Okechukwu J. Obulezi,
Department of Statistics,
Faculty of Physical Sciences,
Nnamdi Azikiwe University, P. O. Box 5025, Awka,
Nigeria.
E-mail address: oj.obulezi@unizik.edu.ng

and

Ehab M. Almetwally,
Department of Mathematics and Statistics,
College of Science, Imam Mohammad Ibn Saud Islamic University (IMSIU), Riyadh 11432,
Saudi Arabia.
E-mail address: emalmetwally@imamu.edu.sa

and

Mohammed Elgarhy,
Faculty of Computers and Information Systems,
Egyptian Chinese University,
Egypt;

Department of Computer Engineering,
Biruni University, 34010, Istanbul,
Turkey.
E-mail address: dr.moelgarhy@gmail.com